

## Classification of precursors in nanoscale droplets

Rolf E. Isele-Holder\* and Ahmed E. Ismail†

*Aachener Verfahrenstechnik: Molecular Simulations and Transformations and AICES Graduate School,  
RWTH Aachen University, Schinkelstraße 2, 52062 Aachen, Germany*

(Received 1 March 2016; published 22 April 2016)

Molecular precursors, ultrathin films that precede spreading droplets, are still far from being understood, despite intensive study. The inherent microscopic length scales make small-scale experimental techniques and molecular simulation ideal methods to study this phenomenon. Previous work on molecular precursors using nanoscale droplets, however, consistently suffers from incorrect measurement of the dimensions of the precursor film. An alternative method to accurately characterize the precursor film is presented here. In contrast to previous measures, this method (i) allows for easy detection and characterization of precursors and (ii) yields wetting dynamics that agree with experimental observations. Finally, we briefly comment on previous studies whose conclusions may merit reconsideration in light of the present work.

DOI: [10.1103/PhysRevE.93.043319](https://doi.org/10.1103/PhysRevE.93.043319)

### I. INTRODUCTION

The slow-spreading kinetics of liquid droplets is controlled by the enormous viscous dissipation that occurs in the immediate vicinity of the contact line [1]. In fact, continuum theories, if invoked with no-slip boundary conditions and a sharp leading droplet edge, predict logarithmically diverging viscous dissipation [2]. This paradox of infinite viscous dissipation is avoided by mechanisms at the contact line, such as evaporation and condensation [3], diffusive interfaces [4], slip between the droplet and the substrate [2,5], or precursor films of molecular thickness [6]. Precursor films can evolve in various shapes, such as layers of constant thickness, continuously growing precursors, or distinct layers [7,8]. Because molecular precursors can control the macroscopic spreading kinetic of liquids, they are of general interest in the wetting community and have gained attention in numerous studies [9,10]. These research efforts have led to significant progress in understanding the mass transport mechanisms and dynamics of wetting. Requirements for the existence of precursors or even the shapes of precursors, however, are still not fully understood [10].

Continuum theories on molecular precursors [11,12] fail to capture the apparently universally valid, experimentally observed diffusive spreading kinetics [10],

$$l = \sqrt{Dt} = (Dt)^\alpha, \quad (1)$$

where  $l$  is the precursor length,  $D$  is a diffusion coefficient,  $t$  is the time, and  $\alpha = 0.5$  is the spreading exponent. Only microscopic theories are able to capture this feature successfully [13,14]. It is therefore obvious that nanoscale experimental and simulation techniques, which are able to resolve microscopic

scales, will play an important role in further investigation and understanding of molecular precursors.

Nanoscale techniques, and in particular molecular simulations, have already been applied to study precursors in numerous studies summarized in Refs. [9,10]. Reviewing this work, however, we found that essentially all of these studies suffer from an incorrect characterization of the precursor. The correct definition of the precursor length is the distance  $l$  from the tip of the precursor to the beginning of the macroscopic part of the droplet, as shown in Fig. 1. All molecular simulation studies on molecular precursors of spreading droplets that we are aware of [9,15–41], however, have consistently measured, analyzed, and reported results for the distance of the precursor tip to the center of the droplet  $r$ . It is noteworthy that the problem of incorrect precursor definition is naturally avoided for other spreading scenarios, such as the formation of precursors in capillaries [42,43].

In this work, we present an analysis method to measure and characterize precursors in molecular simulation and demonstrate its benefits over previously used, incorrect analysis methods. Details of the spreading simulations to which we apply the method are given in Sec. II. The method for characterizing the precursor is presented in Sec. III. The benefits of the analysis method are presented in Sec. IV. There we also discuss findings from previous studies that should be reconsidered based on the work presented here. We offer our conclusions in Sec. V.

Before proceeding, a brief comment on why previous studies used incorrect measurements of the precursor length is in order. Most experimental studies, in which the droplets are large and the exact definition of the precursor films therefore does not seem to play a dominant role, use  $r$  as the length of the precursor. It is rarely reported in the literature that the actual length of the precursor is the distance  $l$  from the precursor tip to the macroscopic droplet edge, and such reports only appeared years after the incorrect measurement of precursors was entrenched in molecular simulations [10,44,45].

### II. SPREADING SIMULATIONS

We use molecular dynamics (MD) to simulate the spreading of a cylindrical droplet on a crystalline substrate. Cylindrical

\*Present address: Theoretical Soft Matter and Biophysics, Institute of Complex Systems and Institute for Advanced Simulation, Forschungszentrum Jülich GmbH, 52425 Jülich, Germany; [isele@aices.rwth-aachen.de](mailto:isele@aices.rwth-aachen.de)

†Present address: Department of Chemical and Biomedical Engineering, P.O. Box 6102, Morgantown, WV, 26506-6102; [aei@alum.mit.edu](mailto:aei@alum.mit.edu); [ahmed.ismail@mail.wvu.edu](mailto:ahmed.ismail@mail.wvu.edu)

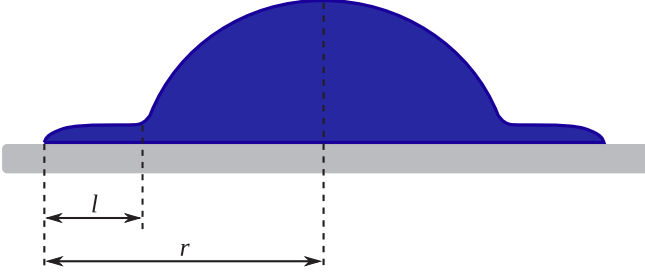


FIG. 1. Sketch of a liquid droplet with a precursor film (blue/dark gray) on a solid substrate (gray/light gray). The distance  $l$ , from the edge of the main droplet to the leading edge of the precursor, is the correct measure for characterizing the precursor length. Previous studies have instead used the distance  $r$  from the leading edge of the precursor to the center of the droplet.

droplets show the same physical behavior as spherical droplets when the different geometries are accounted for properly [31], but have the benefit of being computationally less demanding for the same droplet radius. The substrate is treated explicitly instead of using a continuum approach because it provides a more realistic description of the friction between the droplet and the substrate and also accounts for the ordering of the liquid close to the substrate caused by the structured solid [24]. Modeling the substrate explicitly has the disadvantage of increasing the number of simulated particles and thus the computation time. For cylindrical droplet geometries, however, the ratio of solid to liquid particles is much lower than for spherical simulation setups. The computational overhead thus becomes more tolerable. Our simulation setup is such that the axis of the cylinder points in the  $y$  direction and the normal to the substrate surface points in the  $z$  direction. Spreading, therefore, occurs in the  $x$  direction. Periodic boundary conditions are applied in all directions.

All data are reported with respect to a reference energy  $\epsilon$ , mass  $m$ , distance  $\sigma$ , and a derived time unit  $\tau = (m\sigma^2/\epsilon)^{1/2}$ . Interactions between any two beads  $i$  and  $j$  are described with the Lennard-Jones (LJ) potential,

$$U_{\text{LJ}} = 4\epsilon_{ij} \left[ \left( \frac{\sigma_{ij}}{r_{ij}} \right)^{12} - \left( \frac{\sigma_{ij}}{r_{ij}} \right)^6 \right], \quad (2)$$

where  $r_{ij}$  is the distance between the beads,  $\epsilon_{ij}$  is the depth of the potential well, and  $\sigma_{ij}$  is the distance at which the potential passes through zero, which can roughly be thought of as the bead diameter. For the substrate-substrate interactions we use  $\epsilon_{ss} = 5\epsilon$  and  $\sigma_{ss} = \sigma$ , which provides a stable solid at the simulated temperature. The liquid-liquid interactions are described with  $\epsilon_{ll} = \epsilon$  and  $\sigma_{ll} = \sigma$ . For the solid-liquid interactions, we use  $\sigma_{sl} = \sigma$ . The value of  $\epsilon_{sl}$  is varied in the simulations to control the solid-liquid attraction. To ensure low volatility, the liquid is modeled as linear chains, each chain consisting of 20 beads connected via a FENE potential [46],

$$U_{\text{FENE}} = -0.5kr_0^2 \ln \left[ 1 - \left( \frac{r_{ij}}{r_0} \right)^2 \right], \quad (3)$$

where  $r_0$  is the maximum possible length of a bond and  $k$  is a force constant. We use  $k = 30\epsilon/\sigma^2$  and  $r_0 = 1.5\sigma$ . The

substrate beads have a reduced mass  $m_s = 2m$  and the liquid beads  $m_l = m$ .

The substrate and droplet are prepared and equilibrated separately. The substrate is composed of eight layers of a face-centered cubic crystal with a unit length of  $1.5874\sigma$ . The surface normal pointing in the  $z$  direction is the (111) vector. The substrate dimensions are approximately  $600\sigma \times 33\sigma$  in the  $x$  and  $y$  directions. The lowermost layer of the substrate is held rigid in all simulations. After generating the substrate in an ideal crystal configuration, the substrate is equilibrated at  $T = \epsilon/k_B$  using a Langevin thermostat [47] with damping factor  $\tau_D = 0.3\tau$ . PACKMOL [48] was used to build the initial configuration of a droplet with 9 000 chain molecules. The droplet was preequilibrated for  $500\tau$  at a reduced temperature  $T = \epsilon/k_B$  using a Nosé-Hoover thermostat [49] with damping factor  $\tau_T = 0.5\tau$ .

After the equilibration the droplet was positioned above the substrate such that the minimum distance between substrate and droplet is  $2.5\sigma$ . From then on, only the lower five substrate layers above the rigid layer are coupled to a Langevin thermostat [47] with a damping factor  $\tau_d = 0.3\tau$  to act as a heat sink. The rest of the material is not coupled to a thermostat and therefore obeys Newton's equations of motion.

A two-stage rRESPA integrator [50] is used to integrate the equations of motion. Bonded interactions and nonbonded interactions within a distance of  $3.0\sigma$  that are shifted to zero starting at  $2.5\sigma$  are computed with a frequency of  $0.005\tau$ . A PPPM solver with  $i\mathbf{k}$  differentiation, interpolation order  $P = 5$ , grid spacing  $h \approx 0.75\sigma$ , Ewald parameter  $\beta = 1.0/\sigma$ , and a real-space cutoff  $r_c = 3.0\sigma$  is used to compute long-ranged dispersion interactions [51,52]. All simulations were performed with the LAMMPS MD package [53].

### III. PRECURSOR CHARACTERIZATION

A method for characterizing precursors must provide three features. First, it must correctly determine if a precursor forms. Second, it must provide information about the correct length of the precursor  $l$ . Third, it must identify the precursor type (e.g., terraced or continuously growing). The approach of the method presented here is to first define layers of the droplet. The length  $l_i$  of each layer  $i$  ahead of the droplet is defined in a second step. Finally, a method similar to experimental ellipsometry measurements is used in a third step to characterize the precursor type. The entire process is visualized in Figs. 2 and 3.

#### A. Layer definition

The identification of layers is done with the same approach used in one of the first MD studies on precursors [24]. Near a solid wall, such as the substrate in our simulations, liquid particles are more ordered compared to the bulk liquid and form layers of molecular thickness. The separation of these layers can easily be determined from density profiles of the liquid in the  $z$  direction, as shown in Fig. 2. For small values of  $z$ , the profile oscillates, with each peak corresponding to a molecular layer. The position of the minima are used to separate different layers. The oscillations decay with increasing distance from the substrate. Defining discrete layers

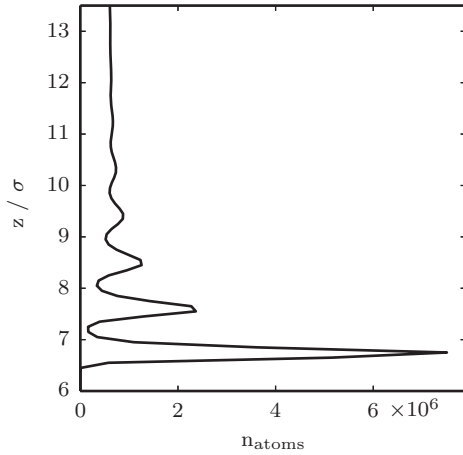


FIG. 2. Number count of liquid particles as a function of  $z$ . Close to the substrate, there is a natural layering of the atoms, each corresponding to one molecular layer.

is not possible for larger distances, but is also not required because the relevant processes for molecular precursors occur close to the substrate.

### B. Layer length computation

The next step is to define the length  $r$  of each molecular layer. Previous approaches approximated the length of a layer as (i) the distance between the minimum and maximum extrema of the particles [25], (ii) the number of particles included in that layer [27,28], or (iii) the point where the local binned density drops below a specified threshold [22,23]. The first approach obviously fails if single molecules separate from the droplet and spread far ahead of the contact line and the rest of the precursor. The second approach is more stable, but changes in the local density of the precursor, such as those reported in Ref. [24], cannot be captured by this method. The last approach compensates for this weakness, but the position of the interface can only be resolved to the width of the bins used to create the histograms of the densities. To overcome these shortcomings, we use an alternative approach to determine the length of each layer. For a given snapshot, the particles are binned in a histogram in the  $x$  and  $z$  directions. For small  $z$ , the bins are separated according to the separation of layers; for large  $z$ , where layering is not visible, the bins are separated by a distance  $\sigma$ . The width of the bins in the  $x$  direction is uniformly taken as  $\sigma$ . Each horizontal layer of the histogram is fit to an error function. The inflection point of the error function is used as the position of the liquid-vapor interface, which for the lowest layers corresponds to the tip of the precursor, as shown in Figs. 3(b) and 3(c).

The final step in the analysis is to determine the length of the precursor for each layer. As mentioned above, previous studies have incorrectly measured the precursor length as the distance from the precursor tip to the center of the droplet, whereas the length from the tip of the precursor to the macroscopic part of the droplet is the correct measure [10]. To define this distance, we fit a circular arc to the positions of the interface of the 20 upper layers, where 20 was chosen to provide good fits to the macroscopic droplet shape while avoiding inclusion of

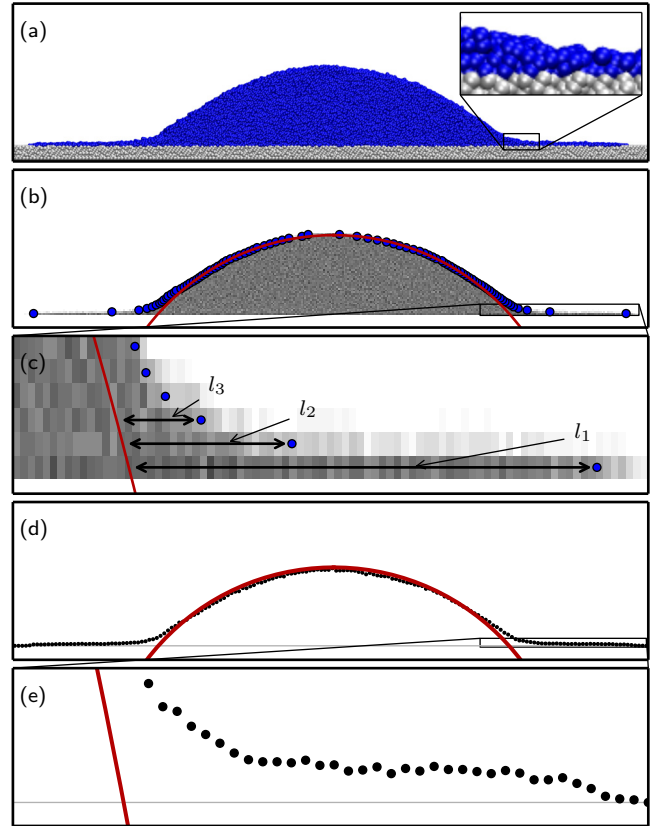


FIG. 3. Characterization of the precursor: (a) Snapshot from a simulation with a thin precursor. The inset shows a selected area of the precursor. From the image, it is difficult to judge if the change in the precursor height is continuous or stepwise. (b) Histogram of the density of the droplet. The blue (dark gray) points denote the position of the interface. The red (medium gray) line is the circular arc fitted to the data points. (c) Close-up of the precursor with unequal scaling in  $x$  and  $z$  direction for clarity.  $l_1$ ,  $l_2$ , and  $l_3$  are the length of the first three precursor layers. (d) The black points denote the effective height of the droplet as obtained from ellipsometry measurements. The red (medium gray) line is the circular arc obtained from a fit to the measured interface positions. The light-gray line corresponds to the base position of the surface. (e) Close-up to the contact line region with unequal scaling in  $x$  and  $z$  directions for clarity. The measurement reveals that the precursor is continuously growing and not terraced [as might be inferred from (a)].

the region close to the foot, which can show strong deviations from the spherical droplet shape. The horizontal distance of the liquid-vapor interface to the circular arc is the precursor length  $l_i$  of layer  $i$ , as shown in Figs. 3(b) and 3(c). The horizontal distance to the liquid-vapor interface to the center of the drop (the incorrect value for the layer length used in previous studies) is denoted as  $r_i$  in the following.

### C. Precursor-shape characterization

The layer length  $l_i$  can be used to identify whether a precursor develops. If multiple layers separate from the droplet, however, it does not provide information whether the precursor is continuously growing or evolves in distinct layers. In previous simulation studies, the precursor type has

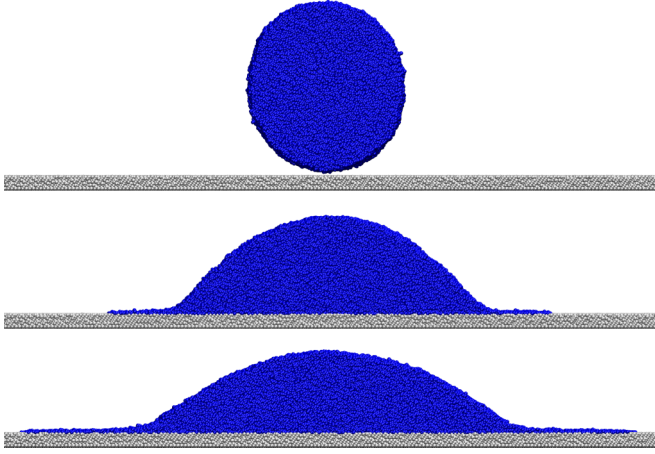


FIG. 4. Spreading of the liquid droplet (blue/dark gray) on the substrate (light gray) with  $\epsilon_{sl} = 1.5\epsilon$  at times (from top to bottom)  $0\tau$ ,  $4550\tau$ , and  $10\,500\tau$ . A thin precursor evolves.

usually been identified from simulation snapshots. As shown in Fig. 3(a), however, this approach is unreliable and has lead to conflicting claims for the observed precursor shape for nearly identical models. In particular, D’Ortona *et al.* [28] claim the observation of a terraced precursor, whereas Heine *et al.* claim the observation of a single-layer precursor for a very similar model [22]. Additional analysis is thus required to fully characterize the precursor.

We characterize the precursor type by a measure that mimics experimental ellipsometry techniques. Ellipsometry measurements provide an effective thickness of the liquid that can, for a dilute layer, be smaller than the molecular diameter [10] and corresponds to the average number of fluid particles per substrate area. This quantity can be approximated in simulations by binning the particles in the  $x$  direction only and counting the number of particles in each bin. This data is then multiplied by a constant such that the maximum value of the histogram corresponds to the height of the droplet at its center. The resulting data is similar to the results obtained from ellipsometry measurements and can be used as an auxiliary tool to differentiate precursor types, as shown in Figs. 3(d) and 3(e).

## IV. RESULTS AND DISCUSSION

After positioning the droplet above the substrate, the long-ranged attractive dispersion interactions pull the droplet to the substrate and the droplet starts to spread. If the solid-liquid interaction energy  $\epsilon_{sl}$  is sufficiently large, a precursor evolves ahead of the main part of the droplet, as shown in Fig 4.

### A. Precursor shape

We now assess the capability of the method to characterize precursors. An overview of the results is given in Figs. 5 and 6. From the simulation snapshots in the left column of Fig. 5 it is immediately apparent that a precursor forms at  $\epsilon_{sl} = 1.5\epsilon$ . For the lower and higher interaction energies  $\epsilon_{sl} \in (1.05, 1.1, 3.0)\epsilon$ , it is clear that the droplet is nonspherical close to the three-phase contact line, but a judgment whether

the observation is a precursor or a foot is difficult, which justifies the necessity for quantitative measures.

The evolution of  $r_i$ , given in the middle column of Fig. 5, provides very limited qualitative information beyond what can already be seen from the simulation snapshots. In particular,  $r_i$  is continuously growing for all four depicted layers, and the decision of whether a layer is part of a precursor, a foot, or the macroscopic part of the droplet can only be inferred from the vertical distance between the lines. The existence of a precursor is obvious from this measure for the intermediate interaction energy  $\epsilon_{sl} = 1.5\epsilon$ . For the higher and lower interaction energies, a clear judgment is not possible.

Finally, the evolution of  $l_i$ , given in the right column of Fig. 5, provides clarity about the existence of a precursor. For  $\epsilon_{sl} = 1.05\epsilon$ , the layer lengths  $l_i$  decay over time. Thus, the liquid that precedes the main part of the droplet is not a precursor (which would expand), but a foot to which the main part of the droplet slowly catches up. For the slightly stronger interaction energy  $\epsilon_{sl} = 1.1\epsilon$ , all  $l_i$  are increasing, so a precursor that separates from the droplet is developing. At  $\epsilon_{sl} = 1.5\epsilon$ , only the first two layers  $l_1$  and  $l_2$  grow in size and are part of a precursor; layers  $l_3$  and  $l_4$  do not separate from the droplet. For the strongest interaction energy  $\epsilon_{sl} = 3.0\epsilon$ , only the first layer  $l_1$  grows over time and is part of the precursor film.

The evolution of  $l_i$  provides information whether a precursor forms. The type of precursor, however, remains inaccessible. In particular, if multiple layers separate from the droplet, as for  $\epsilon_{sl} \in (1.1, 1.5)\epsilon$  it is unclear whether the observed precursor is continuously growing or terraced. This information can be accessed from the effective densities of the droplet shapes given in Fig. 6, which show that the observed precursors are continuously growing and not terraced.

### B. Precursor dynamics

To demonstrate the impact of inaccurate precursor definition, we compute spreading exponents for the growth of the correct and incorrect measures of the precursor length  $l_i$  and  $r_i$ .

For  $r_i$ , the spreading exponent can be determined by fitting a function of the type

$$f_r = C(t - t_0)^{\alpha_r} \quad (4)$$

to the measured data, where  $C$  is a coefficient,  $t_0$  is a reference time that needs to be subtracted from the results because the position of  $t = 0$  is not defined in the simulation, and  $\alpha_r$  is the spreading exponent. The parameters  $C$ ,  $t_0$ , and  $\alpha_r$  are determined from the fit. The fit is performed using orthogonal distance regression.

Figure 7 shows the time evolution of the tip-to-center distance of the first layer above the substrate  $r_1$  for varying  $\epsilon_{sl}$ . In addition to the measured data, depicted as points, the plot contains the fitted functions as continuous curves. The fit is excellent for droplets both in the regimes without a precursor ( $\epsilon_{sl} = 1.0\epsilon$ ) and with a precursor (all other lines). The spreading exponents that result from the fit are depicted in the bottom image of Fig. 7 as a function of the solid-liquid interactions  $\epsilon_{sl}$ . With increasing substrate energy, the measured spreading exponents of  $r_1$  increase, reach a maximum of

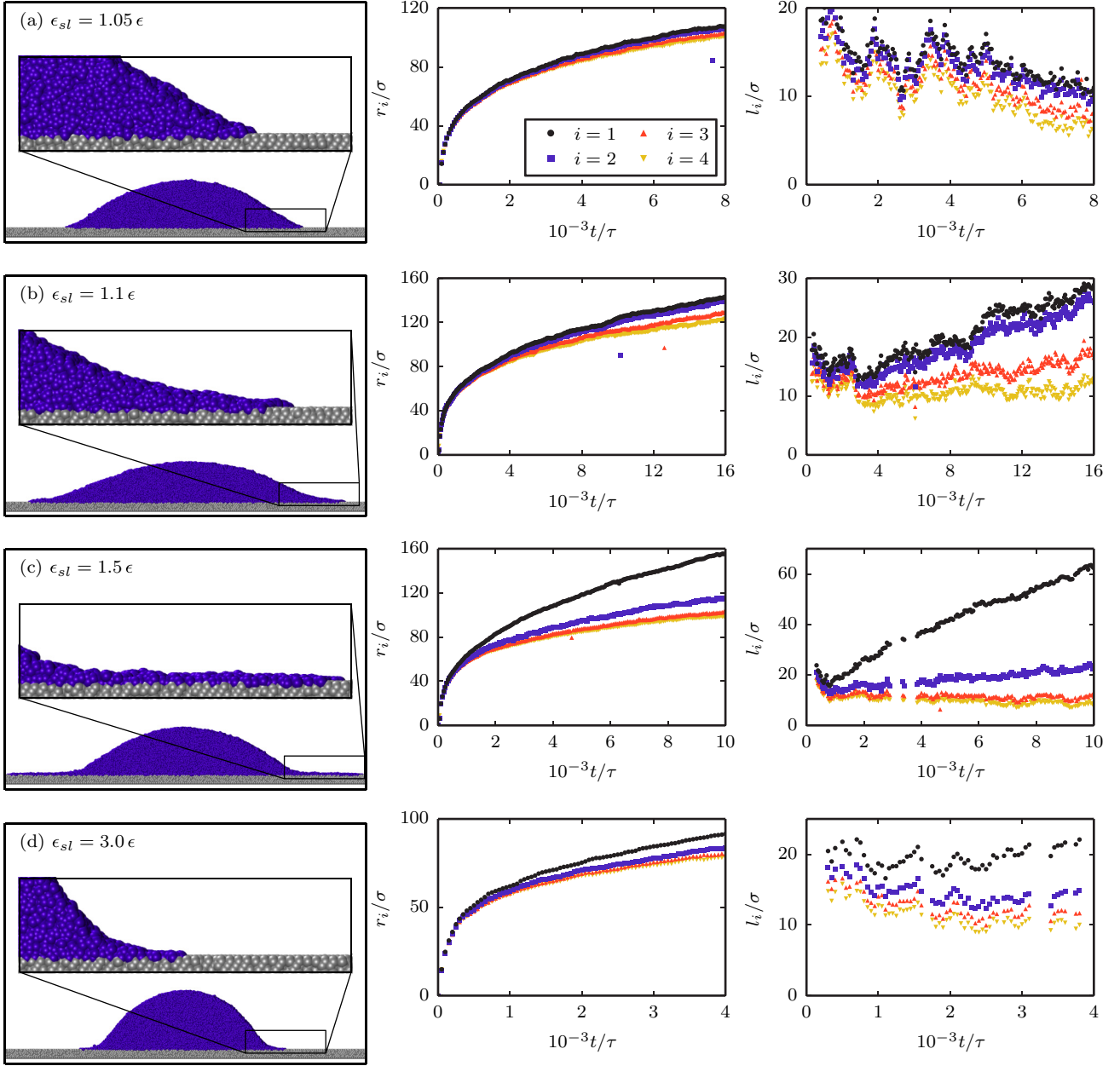


FIG. 5. Left: Visualization of the final snapshots from simulations. Center: Evolution of the length of the first four  $r_i$ . Right: Evolution of the length of the first four  $l_i$ . Rows correspond to different values of  $\epsilon_{sl}$ , as given in the upper left of each row.

$\alpha_r \approx 0.4$  for  $\epsilon_{sl} = 1.3\epsilon$ , and then start to decrease. The measured spreading exponent is neither constant nor is it close to the exponent of 0.5 expected for diffusive spreading. The good agreement between the fit and the measured data suggests that the specified spreading exponents are accurate. These results show that the evolution of  $r_i$  does not necessarily have a spreading exponent of 0.5. That diffusive growth was reported in previous simulation studies for  $r$  might be a coincidence or may indicate that the spreading exponents were not measured carefully enough.

For the correct measure of the precursor length  $l_i$ , the spreading exponents are more difficult to determine.  $l_i$  is computed using the difference between the tip of the drop and the width of the circular arc at the  $z$  position of the layer  $i$ . Because of this, data for  $l_i$  are subject to strong

noise. Moreover, the growth of  $l_i$  is slower than that of  $r_i$ . As a consequence, determining the spreading exponent  $\alpha$  for this data as above for the incorrect measure  $r_i$  is infeasible. Instead, we determine  $\alpha$  as the slope of a linear fit to the log-log representation of the data. The log-log representation of the time evolution of the first layer length  $l_1$  is given in the top image of Fig. 8 for different values of  $\epsilon_{sl}$ . The precursor growth approaches the correct diffusive behavior with increasing simulation time. Note that the precursor growth is fastest for  $\epsilon_{sl} = 1.5\epsilon$ : that is, at intermediate interaction energies. This is in agreement with experimental observations and results from a balance of driving and dissipation forces [18].

The slope of a fitted line to the log-log data provides the spreading exponent. Although performing a linear fit to a

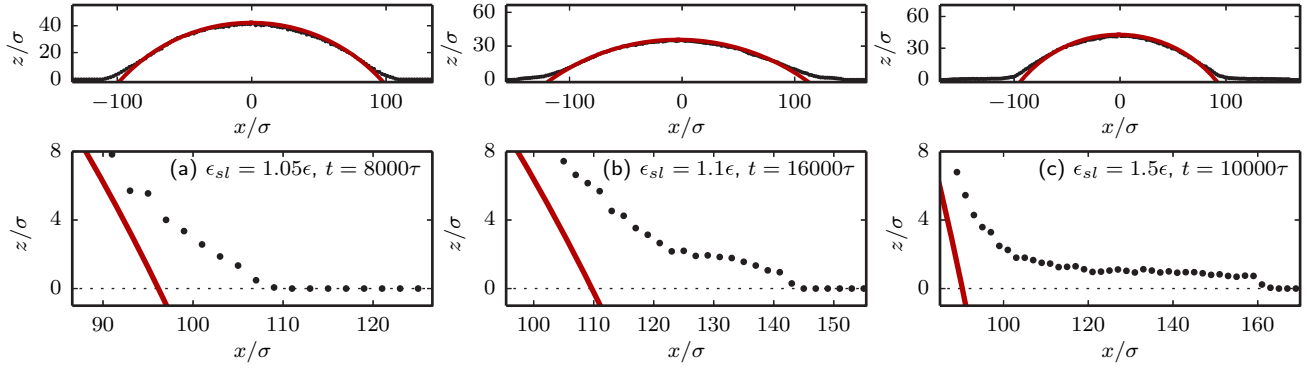


FIG. 6. Effective thickness of the droplet of chain molecules for different values of  $\epsilon_{sl}$ . Top: entire droplet with equal scaling in  $x$  and  $z$  directions. Bottom: selected region with alternate scaling. The snapshots correspond to the final snapshot from each simulation. Multiple distinct layers do not occur in any simulations. While it seems from Fig. 5 that multiple distinct layers separate, results in these images show that the precursor is continuously growing and not terraced.

set of points is numerically trivial, determining the spreading exponent properly is still challenging, because the starting time  $t_0$  is undefined and can impact the results. Moreover, data at the beginning of the simulation is unusable and should be excluded because the precursor has not yet developed. Excluding too

much data, however, restricts the data set too much, and the noise in the data dominates. While we cannot offer a solution to overcome the undefined starting time  $t_0$ , we suggest an approach to handle the amount of data to be included in the fit. To determine how much data should be selected, we performed the fit for different subsets of the data: for each data point of  $l_i$  over  $t$ , we performed a fit such that only the data points at larger values of  $t$  are included, whereas all points at smaller values of  $t$  are excluded. In this way we determine a spreading exponent as a function of  $t$ . For small values of  $t$ , the spreading exponent is influenced by the data from the beginning of the simulation being included. For large  $t$ , the spreading exponent is controlled by the uncertainty caused by the data set being too small. If the approach has worked successfully, the spreading

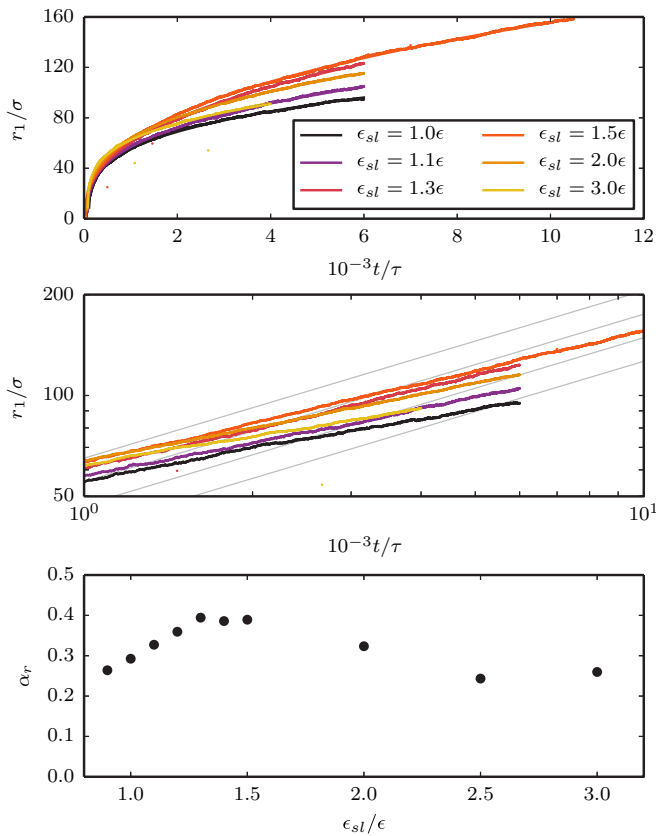


FIG. 7. Top: Measured values of  $r_1$  and fitted functions. Scatter points (that almost look like lines because of their large number): measured data. Continuous lines: fitted functions. Middle: same data in log-log representation. The thin, light-gray lines have a slope of 0.5. Bottom: Spreading exponents  $\alpha_r$  of the first layer as determined from the fit. The spreading exponent for  $\alpha_r$  is smaller than the expected value of 0.5 and not constant.

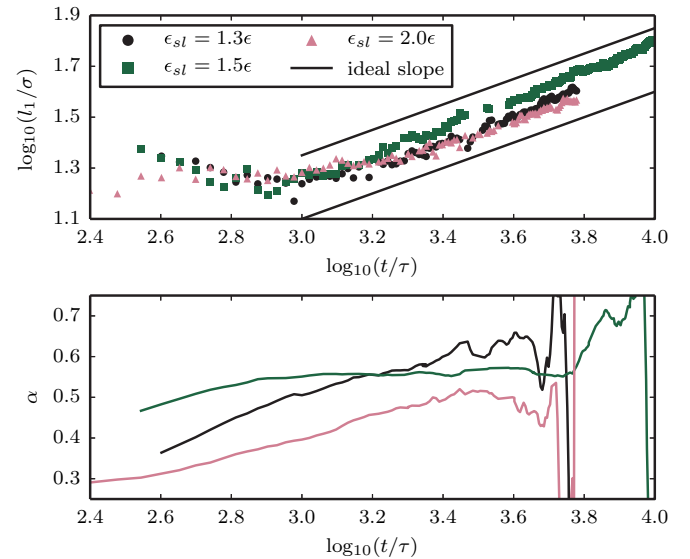


FIG. 8. Analysis of the spreading exponent from the correct measure of the precursor length  $l_1$ . Top: log-log plot of measured data with the ideal slope of 0.5 that matches the diffusive spreading exponent. The measured data approach the diffusive behavior for long simulation times. Bottom: Attempts to measure the spreading exponent from linear fits to the log-log representation. The desired plateau is only observed for  $\epsilon_{sl} = 1.5\epsilon$  and is located at  $\alpha \approx 0.55$ .

coefficients form a plateau for intermediate values of  $t$ . The height of the plateau is an approximate measure of the true spreading exponent.

The resulting curves of the spreading exponents are depicted in the lower plot of Fig. 8.  $\alpha$  forms a plateau for  $\epsilon_{sl} = 1.5\epsilon$ , whereas no plateau is formed for other values of  $\epsilon_{sl}$ . The height of the plateau is approximately  $\alpha = 0.55$ , which is in reasonable agreement with the expected value of 0.5. The remaining difference could result from the starting time  $t_0$  being poorly defined. We would like to point out that the plateau was observed only for this single spreading simulation. All other simulations were thus either too short or the data too noisy to properly quantify the spreading exponent. The correct spreading behavior can only be confirmed from the log-log representation of  $l_1$  for our measurements.

### C. Impact of incorrect analysis

All molecular simulation studies and also numerous experimental studies have used  $r$  to characterize the precursor length. While the findings of most of these studies are presumably not affected by the incorrect choice of measure, there are a couple of conclusions that should be reconsidered in light of the results presented here. First, Heine *et al.* [33] examine the effect of the droplet volume on the spreading dynamics of the precursor and concluded that the diffusion coefficient follows a relation  $D_p \propto R_0^x$ , where  $R_0$  is the initial radius of the droplet in their simulation setup. They report values of  $x = 0.5$  and  $x = 0.65$  for two different systems. These findings are based on the incorrect measure of the precursor length  $r_i$ . That the precursor growth  $l_i$  depends strongly on the droplet size is questionable. That the reservoir size influences the diffusive mass transport of the precursor is implausible and is in conflict with any theoretical model on precursor formation [13,14].

Second, Albrecht *et al.* [54] observed spreading exponents for precursor evolution of 0.12 and 0.14 (i.e., distinctly below the diffusive value of 0.5) in experiments with tiny PDMS droplets with a volume of only a few picoliters. It was argued that the decreased exponents are a result of hindrance of diffusion caused by entanglement of chain molecules [54] or depletion effects caused by the tiny droplet volume [10]. Their findings, however, are based on the incorrect measure  $r_i$  of the precursor length. As shown above, using this incorrect

measure can provide spreading exponents that deviate strongly from 0.5 even when the correct measure for the precursor  $l_i$  exhibits diffusive behavior. Potentially their finding of small spreading exponents is a result of the incorrect measure of the precursor length. Since the experimental length and time scales are still orders of magnitudes larger than in our simulations, however, a direct evaluation of the experimental observations using our simulation results is not possible.

## V. CONCLUSIONS

We suggest an improved approach to characterize precursors in simulations of droplet spreading. Instead of incorrectly measuring the distance from the droplet tip to the droplet center, as done in previous studies, we measure the distance from the droplet tip to the “macroscopic” contact line. In addition, we compute effective densities similar to what is obtained in ellipsometry studies. When combining the results from the evolution of the different layers and the effective densities, a clear identification of the existence and shape of a precursor is possible. Note that both approaches are required to fully describe a precursor. Only using the time evolution of the layers cannot distinguish between continuously growing precursors and terraced layers. Likewise, using the effective densities cannot identify whether a precursor separates or not. A disadvantage of the method seems to be that the determination of the spreading exponents with this approach is difficult because of slower growth and the noise in the data. The slower growth, however, is a feature of the precursors and not the method presented here. The noise in the data is a result of the necessity to obtain  $l_i$  as the difference between two large values and the circular fit to the droplet geometry. A method to reduce this noise in the data is briefly addressed in subsequent work [55].

## ACKNOWLEDGMENTS

We thank Francisco Fontenele and André Bardow for helpful discussions. Financial support for REI from the Deutsche Forschungsgemeinschaft (German Research Foundation) through Grant No. GSC 111 and access to computer resources provided by JARA-HPC are gratefully acknowledged.

- 
- [1] D. Bonn, J. Eggers, J. Indekeu, J. Meunier, and E. Rolley, *Rev. Mod. Phys.* **81**, 739 (2009).
  - [2] C. Huh and L. E. Scriven, *J. Colloid Interface Sci.* **35**, 85 (1971).
  - [3] P. C. Wayner, Jr., *Langmuir* **9**, 294 (1993).
  - [4] P. Seppacher, *Int. J. Eng. Sci.* **34**, 977 (1996).
  - [5] P. A. Thompson and S. M. Troian, *Nature* **389**, 360 (1997).
  - [6] M. Eres, L. Schwartz, and R. Roy, *Phys. Fluids* **12**, 1278 (2000).
  - [7] F. Heslot, N. Fraysse, and A.-M. Cazabat, *Nature* **338**, 640 (1989).
  - [8] A.-M. Cazabat, N. Fraysse, F. Heslot, P. Levinson, J. Marsh, F. Tiberg, and M. P. Valignat, *Adv. Colloid Interface Sci.* **48**, 1 (1994).
  - [9] V. M. Samsonov, *Curr. Opin. Colloid. Interface Sci.* **16**, 303 (2011).
  - [10] M. N. Popescu, G. Oshanin, S. Dietrich, and A.-M. Cazabat, *J. Phys.: Condens. Matter* **24**, 243102 (2012).
  - [11] P.-G. De Gennes and A.-M. Cazabat, *C. R. Acad. Sci.* **310**, 1601 (1990).
  - [12] D. B. Abraham, P. Collet, J. De Coninck, and F. Dunlop, *Phys. Rev. Lett.* **65**, 195 (1990).
  - [13] S. F. Burlatsky, G. Oshanin, A.-M. Cazabat, and M. Moreau, *Phys. Rev. Lett.* **76**, 86 (1996).
  - [14] D. B. Abraham, R. Cuerno, and E. Moro, *Phys. Rev. Lett.* **88**, 206101 (2002).

- [15] J. De Coninck, S. Hoorelbeke, M. P. Valignat, and A.-M. Cazabat, *Phys. Rev. E* **48**, 4549 (1993).
- [16] J. De Coninck, M. Frayasse, M. P. Valignat, and A.-M. Cazabat, *Langmuir* **9**, 1906 (1993).
- [17] J. De Coninck, *Colloid Surface A* **114**, 155 (1996).
- [18] M. Voué, M. P. Valignat, G. Oshanin, A.-M. Cazabat, and J. De Coninck, *Langmuir* **14**, 5951 (1998).
- [19] M. Voué, S. Semal, and J. De Coninck, *Langmuir* **15**, 7855 (1999).
- [20] M. Voué and J. De Coninck, *Acta Mater.* **48**, 4405 (2000).
- [21] M. Voué, S. Rovillard, J. De Coninck, M. P. Valignat, and A.-M. Cazabat, *Langmuir* **16**, 1428 (2000).
- [22] D. R. Heine, G. S. Grest, and E. B. Webb, III, *Phys. Rev. E* **68**, 061603 (2003).
- [23] J.-X. Yang, J. Koplik, and J. R. Banavar, *Phys. Rev. Lett.* **67**, 3539 (1991).
- [24] J.-X. Yang, J. Koplik, and J. R. Banavar, *Phys. Rev. A* **46**, 7738 (1992).
- [25] J. A. Nieminen, D. B. Abraham, M. Karttunen, and K. Kaski, *Phys. Rev. Lett.* **69**, 124 (1992).
- [26] J. A. Nieminen and T. Ala-Nissila, *Phys. Rev. E* **49**, 4228 (1994).
- [27] J. De Coninck, U. D'Ortona, J. Koplik, and J. R. Banavar, *Phys. Rev. Lett.* **74**, 928 (1995).
- [28] U. D'Ortona, J. De Coninck, J. Koplik, and J. R. Banavar, *Phys. Rev. E* **53**, 562 (1996).
- [29] S. Bekink, S. Karaborni, G. Verbist, and K. Esselink, *Phys. Rev. Lett.* **76**, 3766 (1996).
- [30] M. Haataja, J. A. Nieminen, and T. Ala-Nissila, *Phys. Rev. E* **52**, R2165 (1995).
- [31] D. R. Heine, G. S. Grest, and E. B. Webb, III, *Phys. Rev. E* **70**, 011606 (2004).
- [32] E. B. Webb, G. S. Grest, and D. R. Heine, *Phys. Rev. Lett.* **91**, 236102 (2003).
- [33] D. R. Heine, G. S. Grest, and E. B. Webb, III, *Phys. Rev. Lett.* **95**, 107801 (2005).
- [34] N. Sedighi, S. Murad, and S. K. Aggarwal, *Fluid Dynam. Res.* **43**, 015507 (2011).
- [35] C. Wu, T. Qian, and P. Sheng, *J. Phys.: Condens. Matter* **22**, 325101 (2010).
- [36] E. B. Webb, III, G. S. Grest, D. R. Heine, and J. J. Hoyt, *Acta Mater.* **53**, 3163 (2005).
- [37] Y. Sun and E. B. Webb, III, *J. Phys.: Condens. Matter* **21**, 464135 (2009).
- [38] V. M. Samsonov and A. S. Ratnikov, *Colloid Surface A* **298**, 52 (2007).
- [39] V. M. Samsonov, V. V. Dronnikov, A. A. Volnukhina, and S. D. Muravyev, *Surf. Sci.* **532–535**, 560 (2003).
- [40] A. Milchev and K. Binder, *J. Chem. Phys.* **116**, 7691 (2002).
- [41] J. Yaneva, A. Milchev, and K. Binder, *Macromol. Theory Simul.* **12**, 573 (2003).
- [42] S. Chibbaro, L. Biferale, F. Diotallevi, S. Succi, K. Binder, D. Dimitrov, A. Milchev, S. Girardo, and D. Pisignano, *Europhys. Lett.* **84**, 44003 (2008).
- [43] S. Chibbaro, L. Biferale, K. Binder, D. Dimitrov, F. Diotallevi, A. Milchev, and S. Succi, *J. Stat. Mech.: Theor. Exp.* (2009) P06007.
- [44] H. Xu, D. Shirvanyants, K. Beers, K. Matyjaszewski, M. Rubinstein, and S. S. Sheiko, *Phys. Rev. Lett.* **93**, 206103 (2004).
- [45] H. Xu, F. C. Sun, D. G. Shirvanyants, M. Rubinstein, D. Shabratov, K. L. Beers, K. Matyjaszewski, and S. S. Sheiko, *Adv. Mater.* **19**, 2930 (2007).
- [46] K. Kremer and G. S. Grest, *J. Chem. Phys.* **92**, 5057 (1990).
- [47] T. Schneider and E. Stoll, *Phys. Rev. B* **17**, 1302 (1978).
- [48] L. Martínez, R. Andrade, E. G. Birgin, and J. M. Martínez, *J. Comput. Chem.* **30**, 2157 (2009).
- [49] W. Shinoda, M. Shiga, and M. Mikami, *Phys. Rev. B* **69**, 134103 (2004).
- [50] M. Tuckerman, B. J. Berne, and G. J. Martyna, *J. Chem. Phys.* **97**, 1990 (1992).
- [51] R. E. Isele-Holder, W. Mitchell, and A. E. Ismail, *J. Chem. Phys.* **137**, 174107 (2012).
- [52] R. E. Isele-Holder, W. Mitchell, J. R. Hammond, A. Kohlmeyer, and A. E. Ismail, *J. Chem. Theory Comput.* **9**, 5412 (2013).
- [53] S. Plimpton, *J. Comput. Phys.* **117**, 1 (1995).
- [54] U. Albrecht, A. Otto, and P. Leiderer, *Phys. Rev. Lett.* **68**, 3192 (1992).
- [55] R. E. Isele-Holder and A. E. Ismail, *Langmuir* **32** (2016), doi:10.1021/acs.langmuir.6b00807.